

# Configurational Entropy as a tool to select a physical Thick Brane Model

M. Chinaglia<sup>1,\*</sup> W. T. Cruz<sup>2,†</sup> R. A. C. Correa<sup>1,‡</sup> W. de Paula<sup>1,§</sup> and P. H. R. S. Moraes<sup>1,¶</sup>

<sup>1</sup>*ITA, Instituto Tecnológico de Aeronáutica,*

*12228-900, São José dos Campos, SP, Brazil and*

<sup>2</sup>*Instituto Federal de Educação Ciência e Tecnologia do Ceará,*  
*campus Juazeiro do Norte, CE, Brazil*

(Dated: December 14, 2024)

## Abstract

We analyse braneworld scenarios via a configurational entropy (CE) formalism. Braneworld scenarios have drawn attention mainly due to the fact that they can explain the hierarchy problem and unify the fundamental forces through a symmetry breaking procedure. Those scenarios localize matter in a  $(3 + 1)$  hypersurface, the brane, which is inserted in a higher dimensional space, the bulk. Novel analytical braneworld models, in which the warp factor depends on a free parameter  $n$ , were recently released in the literature. In this article we will provide a way to constrain this parameter through the relation between information and dynamics of a system described by the CE. We demonstrate that in some cases the CE is an important tool in order to provide the most probable physical system among all the possibilities.

PACS numbers: 05.45.Yv, 03.65.Vf, 11.27.+d

---

\*Electronic address: chinaglia.mariana@gmail.com

†Electronic address:

‡Electronic address: fis04132@gmail.com

§Electronic address: wayne@ita.br

¶Electronic address: Moraes.phrs@gmail.com

## I. INTRODUCTION

Due to the inability revealed by General Relativity (GR) to accurately describe some cosmological and astrophysical issues [1–5], new theories of gravity have been proposed. Braneworld models are a possibility that have been in vogue in the last decades because when extra dimensions are considered, they lead to modified field equations that can handle some of those issues in a healthy way. For example, brane scenarios allow for neutron star masses around 2 solar masses, in agreement with observations without the requirement of an exotic equation of state [6]. Besides, this scenario could be a proper way to solve the hierarchy problem [7, 8].

Novel analytical models derived in [8] describe the universe through the brane paradigm and have the prerogative of depending on a free parameter  $n$ . Although varying  $n$  leads to different characteristics in comparison to the literature until then, this parameter has never been constrained by any physical approach.

We propose to use the configurational entropy (CE) presented in [9] in some of the novel analytical braneworld models [8] in order to provide a physical constrain on the parameter  $n$ . This analysis will allow us to find the most-likely physical scenario among all possible values that  $n$  can assume. A similar analysis was done in [10] in favor of finding a bound in  $f(R, T)$  theories; in [11] when searching for Information-entropic analysis of Kortewegde Vries solitons in the quarkgluon plasma; in [12] for this analysis in anti-de Sitter black holes and also in [13] when glueball states were considered.

The paper is organized as follows: in Section II we describe the braneworld model in question, in Section III we review the mathematical approach for the CE calculation, in Section IV we present the CE calculation for the brane scenarios, in Section V we discuss the results and, finally, in Section VI we present the conclusions.

## II. BRANE MODELS

Braneworld scenarios were studied through several analytical procedure strategies [14, 15]. Concerning this paradigm, the observable universe is a manifold with (3+1) dimensions supported by a warp factor responsible for matter localization inside the brane.

The braneworld models studied in this paper were derived in [8] where they were associ-

ated with generic solutions of an effective action driven by a real scalar field,  $\phi$ , coupled to the gravity with  $(4 + 1)\text{D}$  such that [14]:

$$S = \int d^4x dy \sqrt{|g|} \left[ -\frac{1}{4}R + \frac{1}{2}\partial_a\phi\partial^a\phi - V(\phi) \right], \quad (1)$$

where  $|g| = \det(g_{ab})$ ,  $R$  is the scalar curvature in 5D,  $a$  varies from 0 to 4 and  $V(\phi)$  is the scalar field potential.

It was chosen a 5-dimensional braneworld scenario, whose interval is expressed by:

$$ds^2 = e^{2A}\eta_{\mu\nu}dx^\mu dx^\nu - dy^2, \quad (2)$$

with  $e^{2A}$  being the warp factor,  $\eta_{\mu\nu}$  is the Minkowski metric,  $\mu, \nu$  run from 0 to 3 and  $y$  is the extra coordinate.

Assuming a dependency of  $\phi$  exclusively on the extra dimensional coordinate  $y$ , the equation of motion for the scalar field arising from the action (1) is given by

$$\frac{d^2\phi}{dy^2} + 4\frac{dA}{dy}\frac{d\phi}{dy} - \frac{d}{d\phi}V(\phi) = 0. \quad (3)$$

By varying the action (1) with respect to the metric, one obtains

$$\frac{3}{2}\frac{d^2A}{dy^2} = -\left(\frac{d\phi}{dy}\right)^2. \quad (4)$$

The warp factor,  $e^{2A}$ , was constrained from an ansatz in [8]. Considering that energy density localized structures demand for a lump-like warp factor behavior, so that matter integrability and localization are assured on the brane, there can be assumed a straightforward identification such as  $e^{2A} = \psi$ , where  $\psi$  is the bell-shaped analytical expression known *a priori*. This assumption leads to [8]

$$A = \frac{1}{2}\ln\psi. \quad (5)$$

A plethora of analytical lump solutions was obtained in [16], generated via cyclic deformation chains (CDC). They were triggered by the solution of the  $\lambda\chi^4$  potential (in addition of other three deformed models). M. Chinaglia, A. Bernardini and R. da Rocha inserted some of the deformed lump solutions as the ansatz for  $\psi$  in Eq. (5) in order to build up novel analytical braneworld scenarios. A complete review of generic deformations can be found, for example, in [17], while the CDC procedure was proposed in [16]. In [17] the deformation

generates a new system in a way such that one increases or decreases the amplitude and width of the defect, without changing the corresponding topological behavior. In [16] the authors derived deformed defects that, in spite of having different amplitudes and widths, can interchange from topological (kink) to non-topological (lump) profiles. Such a behavior can also be seen in [18]. The deformation procedure as well as the lump solutions are quite extensive and do not concern the scope of this work, however we dedicate a consistent review of it in Appendix A.

Since the lump solutions derived in [16] have a dependency on the parameter  $n$ , the brane warp factor also presents such a dependency. Our interest is to make use of the CE [9] as a tool to set the free parameter  $n$ . For this purpose, it is essential to know the brane energy density spectrum. This was also calculated in [8] through the 00-component of the energy-momentum tensor inside the brane derived in [19, 20]:

$$T_{00} = T_0^0 g_{00} = \left[ \left( \frac{d\phi}{dy} \right)^2 - 3 \left( \frac{dA}{dy} \right)^2 \right] e^{2A(y)}. \quad (6)$$

It is also important to stress that from Eq. (4) one can infer that only some values of  $n$  will generate real physical solutions,  $\phi$ , as will be discussed in details in Section V.

We now present the warp factor,  $e^{2A(y)}$ , and the 00 component of the energy-momentum tensor,  $T_{00}(y)$ , for the 4 braneworld models of Ref.[8]. Those will be analyzed via CE in Section IV. Each subsequent model will be referred by the numbers, 1, 2, 3 and 4 following the sequence they are presented. The behavior of their warp factor and matter-energy density are depicted in Figs. 1, 2, 3 and 4.

The first model considered was driven by the *ansatz*<sup>1</sup>:

$$\psi_1 = \frac{-\ln[\cosh[n \tanh(y)] \operatorname{sech}(n)]}{n}, \quad (7)$$

which inserted in Eq. (5) provide the function  $A(y)$  and this enables the energy-momentum calculation:

$$A(y)_1 = \frac{1}{2} \ln \left[ \frac{-\ln[\cosh[n \tanh(y)] \operatorname{sech}(n)]}{n} \right], \quad (8)$$

$$T_{00}(y)_1 = \frac{3}{4} \left[ n \operatorname{sech}(y)^4 \operatorname{sech}[n \tanh(y)]^2 - 2 \operatorname{sech}(y)^2 \tanh(y) \tanh[n \tanh(y)] \right], \quad (9)$$

that are represented in Fig. 1.

---

<sup>1</sup> In order to understand the *ansatz* derivation for all the models, see Appendix A.

### Model 1

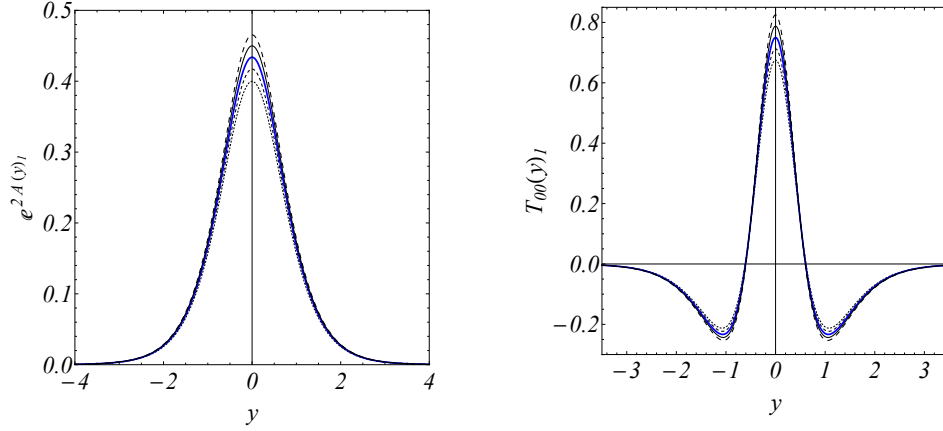


FIG. 1: Brane warp factor and energy-momentum tensor for model 1 derived from  $\psi_1$ .  $n = 1 - 2k; 1 - k, 1, 1 + k, 1 + 2k$   $k = 0.05$ . Blue line represents the solution for  $n = 1$  while black lines ranges from the dotted to the dashed as  $n$  increases.

Fig. 2 presents the second model obtained from the *ansatz*:

$$\psi_2 = \frac{\cos[n \tanh(y)] - \cos(n)}{n}, \quad (10)$$

that generates the scenario with:

$$A(y)_2 = \frac{1}{2} \ln \left[ \frac{-\cos(n) + \cos[n \tanh(y)]}{n} \right], \quad (11)$$

$$T_{00}(y)_2 = \frac{3}{4} \left[ n \cos[n \tanh(y)] \operatorname{sech}(y)^4 - 2 \operatorname{sech}(y)^2 \sin[n \tanh(y)] \tanh(y) \right]. \quad (12)$$

Model 3 has been derived from the *ansatz*:

$$\psi_3 = \frac{(\operatorname{sech}[n \tanh(y)] - \operatorname{sech}(n))}{n} \quad (13)$$

which leads to:

$$A(y)_3 = \frac{1}{2} \ln \left[ \frac{\operatorname{sech}[n \tanh(y)] - \operatorname{sech}(n)}{n} \right], \quad (14)$$

$$T_{00}(y)_3 = -\frac{3}{8} \operatorname{sech}(y)^3 \operatorname{sech}[n \tanh(y)]^3 \times \quad (15)$$

$$[n(-3 + \cosh(2n \tanh(y))) \operatorname{sech}(y) + 2 \sinh(y) \sinh(2n \tanh(y))],$$

whose behavior is depicted in Fig. 3.

Finally, Model 4 was built through the *ansatz*:

$$\psi_4 = \frac{(2n \operatorname{sech}(y) + \sin[2n \operatorname{sech}(y)])}{4n}, \quad (16)$$

### Model 2

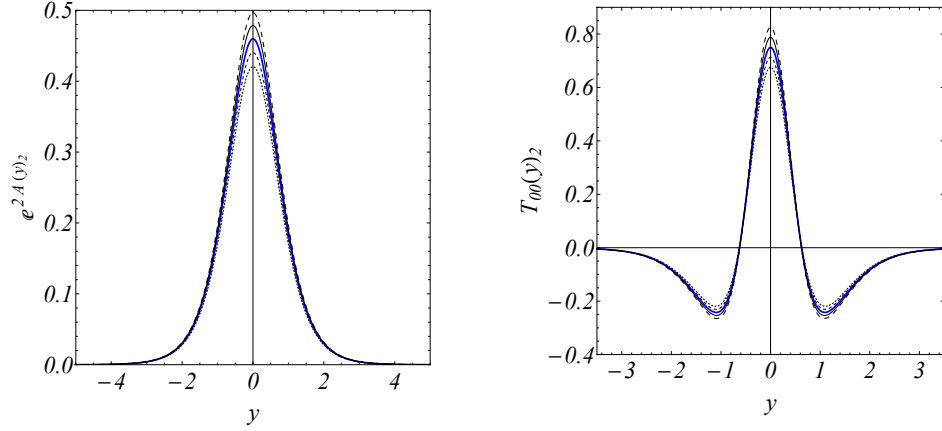


FIG. 2: Brane warp factor and energy-momentum tensor for model 2 derived from  $\psi_2$ .  $n = 1 - 2k; 1 - k, 1, 1 + k, 1 + 2k$   $ek = 0.05$ . Blue line represents the solution for  $n = 1$  while black lines ranges from the dotted to the dashed as  $n$  increases.

### Model 3

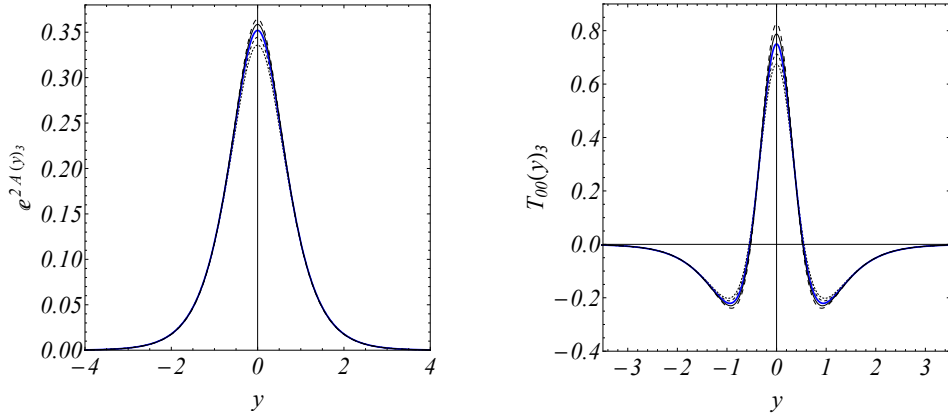


FIG. 3: Brane warp factor and energy-momentum tensor for model 3 derived from  $\psi_3$ .  $n = 1 - 2k; 1 - k, 1, 1 + k, 1 + 2k$   $ek = 0.05$ . Blue line represents the solution for  $n = 1$  while black lines ranges from the dotted to the dashed as  $n$  increases.

that engenders:

$$A(y)_4 = \frac{1}{2} \ln \left[ \frac{2n \operatorname{sech}(y) + \sin[2n \operatorname{sech}(y)]}{4n} \right] \quad (17)$$

$$T_{00}(y)_4 = \frac{3}{4} \operatorname{sech}(y) [\cos(n \operatorname{sech}(y))^2 \operatorname{sech}(y)^2 + \tanh(y)^2 (-\cos[n \operatorname{sech}(y)]^2 + n \operatorname{sech}(y) \sin[2n \operatorname{sech}(y)])]. \quad (18)$$

as can be seen in Fig. 4.

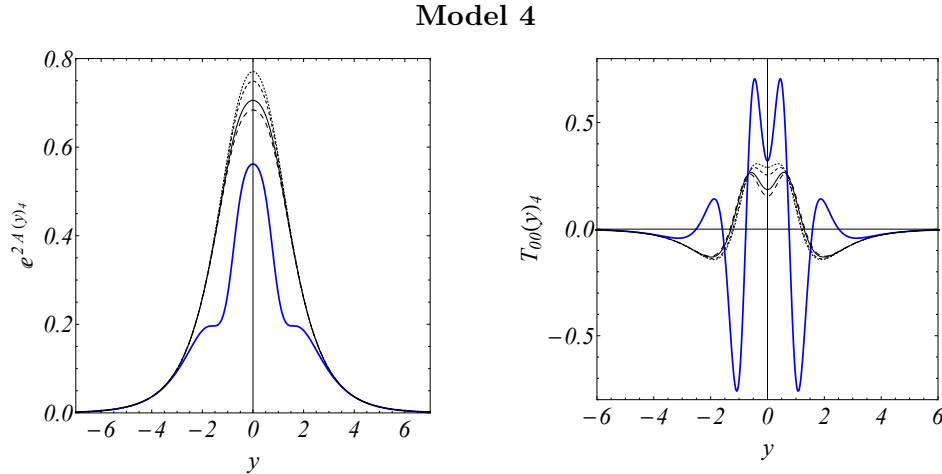


FIG. 4: Brane warp factor and energy-momentum tensor for model 4 derived from  $\psi_4$ .  $n = 1 - 2k; 1 - k, 4, 1 + k, 1 + 2k$   $ek = 0.05$ . Blue line represents the solution for  $n = 4$  while black lines ranges from the dotted to the dashed as  $n$  increases.

### III. CONFIGURATIONAL ENTROPY

The CE procedure was defined in [9] where scalar fields with localized energy profiles were analyzed. CE is a measure of the information content of physical solutions and their approximations. The latter concern to small variations in the real path followed, that arrives from the minimization of some action. The approximations are the CE in the phase space. The analysis here will be done via a relative entropy (RCE), defined through a trial function assumption such that it is the absolute difference between the CE of the real solution and the CE of the trial function (CET).

In the present work the study was developed considering the energy density expressions derived for the brane scenario. We have calculated the CE for trial functions (that are approximations for the real function) in order to use the RCE to find a bound in the model. We show that the RCE is related to the energy of trial functions and that the coarser the approximation, the greater the energy and the CE.

The constraining on the free parameter  $n$  of the brane models under consideration via this formalism is directly related to the minimization of both quantities: the energy of trial functions and the RCE. Therefore, we have found a properly way to pick the best scenario

via a quite original tool: the RCE. As evinced in [9], nature is the ultimate optimizer, for it will maximize energy considering both perspectives: the dynamical and the informational one.

In this section, we present a review of the CE calculation, which is completely described in [9].

Considering the brane localized energy density pattern, it is possible to write the following relation:

$$\int_{-\infty}^{+\infty} |\rho(x)|^2 dx = \int_{-\infty}^{+\infty} |P(k)|^2 dk, \quad (19)$$

where the density  $\rho(x)$  is the weight of some  $k$  mode and

$$\rho(k) = \frac{|P(k)|^2}{\int |P(k)|^2 d^d k}. \quad (20)$$

If the functions are periodic, they can be written as Fourier series. In this case, each squared term represents the probability of occurrence of the  $k$  mode, such that  $\rho(k) \rightarrow \rho_n = |A_n|^2 / \sum |A_n|^2$ .

We define the CE as:

$$S_C[\rho] = - \sum \rho_n \ln(\rho_n). \quad (21)$$

Note that Eq. (21) is analogue to the Shannon informational entropy, which represents a limit for the best way to compactify information without losses [21]. Besides, note that both Eq. (21) and Shannon's entropy are also analogue to the usual thermodynamical entropy described by Boltzmann equation,  $S = -Rf \ln(f)$ , considering the Stirling approximation:  $\ln f! = f \ln f$ . Here,  $f$  is the frequency of some event divided by the number of total events. As it is defined, CE provides the informational content of the possible configurations compatible with the constraints of the physical system. If there are constraints on the system, a shorter amount of information is reacquired. If there is no constraint, the system is completely aleatory and all the information will be relevant.

In order to find such constraints, Shannon defined a redundancy factor in terms of a maximum entropy value. This maximum condition is attained when the uncertainty of the event is also maximal (completely aleatory event), so that the informational content intrinsic to each event is higher. In order to acquire a maximum value of uncertainty, one must have the most equal distribution as possible for the frequency associated to each event. That is, all the events must have the same probability, so that the entropy will be maximized.



In a similar way, here it will be chosen a maximum entropy in order to find the constraints in the brane scenario. When all the  $N$   $k$  modes carry the same weight (i.e., the same probability), the CE is maximum. By doing this, we will be able to compare both the real and the maximum entropy to find the constraints and, consequently, the redundancy. We will then constrain the free parameter  $n$ . Consequently, this work will provide a physical observable, the entropy, which is capable of selecting the most probable physical model.

Note that, even if the function has any periodicity, it is still possible to define the CE:

$$S_c[\rho] = - \int \tilde{\rho}(k) \ln[\tilde{\rho}(k)] d^d k \quad (22)$$

In the next Section we calculate the CE for the brane model presented in Section II.

#### IV. CONFIGURATIONAL ENTROPY FOR THE BRANE SCENARIOS

In this section we evaluate the CE resulting from each brane model presented in Sec. II. In order to achieve the modal fraction (20), we need to know the energy density along the extra dimension. Due to the complexity of the solutions for  $T_{00}(y)$ , we numerically calculate the Fourier transform and from there we obtain the modal fraction. To finally obtain the CE from Eq. (22) we define the normalised modal fraction as  $\tilde{\rho}(k) = \rho(k)/\rho_{max}(k)$ . The integration region to the CE in Eq. (22) is chosen so that at its limits we obtain  $\tilde{\rho}(k) \ln[\tilde{\rho}(k)] \rightarrow 0$ . Our results are presented as the plots of the CE in terms of the parameter  $n$  in each case. For convenience we choose the warp factor so that  $e^{2A(0)} = 1$ . Then, we adopt  $\tilde{A}(y) = A(y) - A(0)$  and find new expressions for  $\rho(y)$ .

For Model 1, we obtain the following energy density from the normalized warp factor  $\tilde{A}(y)$ :

$$\rho(y)_1 = - \frac{3n \operatorname{sech}(y)^3 [n \operatorname{sech}(y) \operatorname{sech}[n \tanh(y)]^2 - 2 \sinh(y) \tanh[n \tanh(y)]]}{4[\ln \operatorname{sech}(n)]}. \quad (23)$$

The corresponding CE is presented in Fig. 5. The lowest value obtained for the CE was 2.0665. When  $n$  acquires large values, the CE tends to 5.8331.

For Model 2 we find the following energy density with the normalized warp factor:

$$\rho(y)_2 = - \frac{3n \operatorname{sech}(y)^3 [n \cos[n \tanh(y)] \operatorname{sech}(y) - 2 \sin[n \tanh(y)] \sinh(y)]}{4[-1 + \cos(n)]}. \quad (24)$$

The corresponding CE is plotted in Fig. 6.

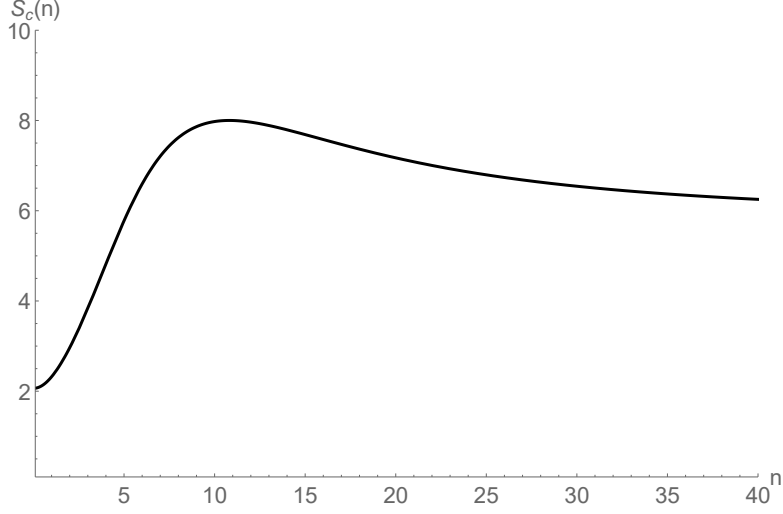


FIG. 5: CE for the Model 1 with  $0.1 \leq n \leq 40$ . The minimum CE is 2.0665 at  $n = 0.1$  and the maximum CE is 8.0008 at  $n = 10.8161$ .

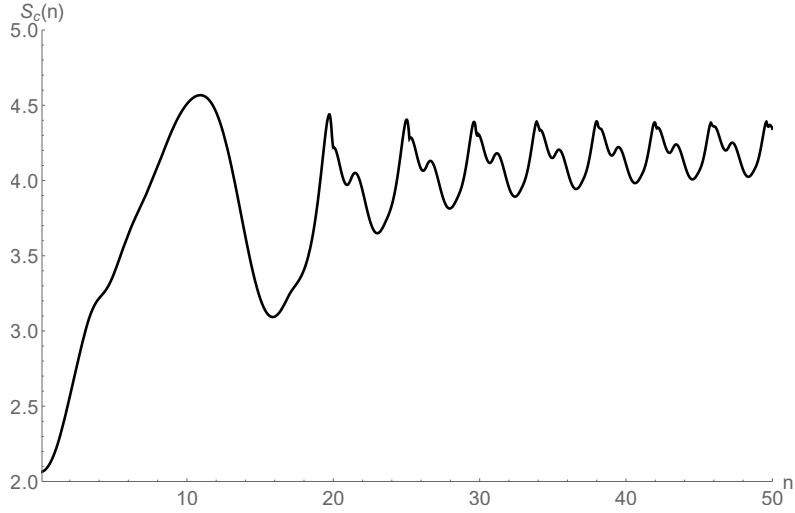


FIG. 6: CE for the Model 2 with  $0.1 \leq n \leq 50$ . The minimum CE is 2.0651 at  $n = 0.1$  and the maximum CE is 4.5671 at  $n = 10.9191$ .

The Model 3 have the following energy density:

$$\rho(y)_3 = [n(-3 + \cosh[2n \tanh(y)]) \operatorname{sech}(y) + 2 \sinh(y) \sinh[2n \tanh(y)]] \times \frac{3n \operatorname{sech}[y]^3 \operatorname{sech}[n \tanh(y)]^3}{8[1 - \operatorname{sech}(n)]}, \quad (25)$$

and its corresponding CE is plotted in Fig. (7).

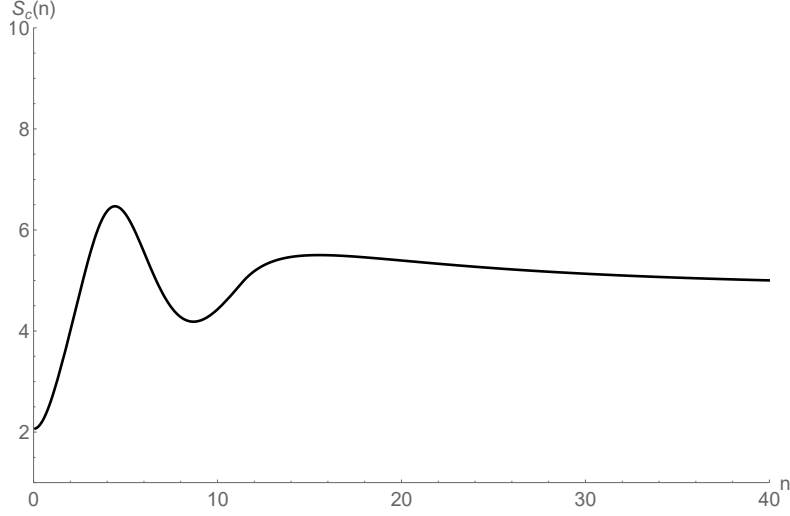


FIG. 7: CE for the Model 3 with  $0.1 \leq n \leq 40$ . The minimum CE is 2.0706 at  $n = 0.1$  and the maximum CE is 6.4687 at  $n = 4.4245$ .

At last, the energy density coming from the normalized warp factor for Model 4 is

$$\rho(y)_4 = \frac{3n \operatorname{sech}(y)^3 [-\cos[n \operatorname{sech}(y)]^2 (-1 + \sinh(y)^2) + n \sin[2n \operatorname{sech}(y)] \sinh(y) \tanh(y)]}{[2n + \sin(2n)]}, \quad (26)$$

and the resulting CE is presented in Fig. 8.

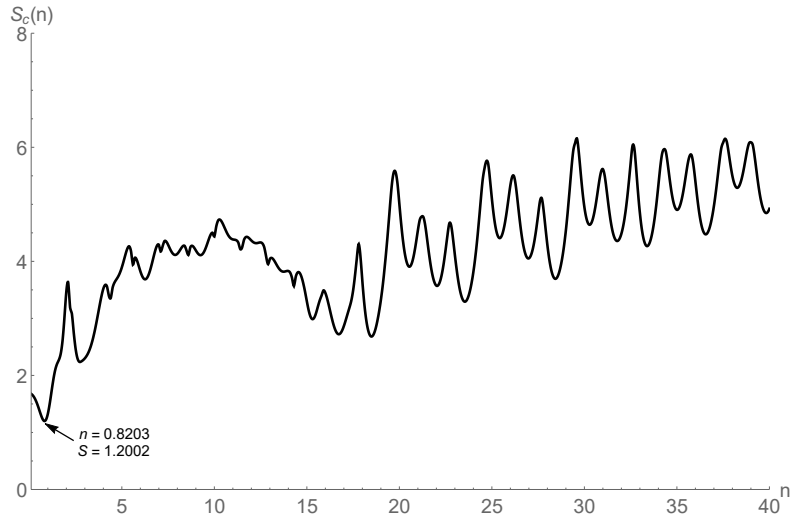


FIG. 8: CE for the Model 4 with  $0.1 \leq n \leq 40$ . The minimum CE is 1.2002 at  $n = 0.8203$ .

For the four models analysed we have started the CE numerical evaluation considering  $n = 0.1$  with 0.1 steps. The Models 1, 2 and 3 have presented smaller CE values at the

minimum  $n$  adopted. In these cases, the models have presented close CE minimum values. In addition, the brane scalar fields behavior relative to those three models for the minimum CE are very similar and we present the behavior of Model 1 in Fig. 9. Model 4 presents the minimum CE at  $n = 0.8203$  and has a different behavior which becomes prominent when we consider greater values of  $n$ , as shown in Fig. 10.

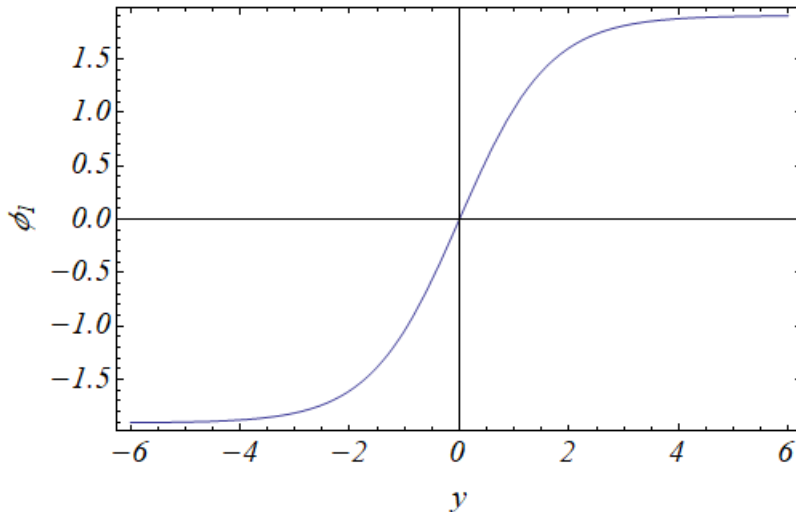


FIG. 9: Brane scalar field relative to Model 1 considering  $n = 0.1$ . The models 2 and 3 present a very similar qualitative and quantitative behavior.

## V. TACHYONIC SOLUTIONS

For a given warp factor one can analyze if the scalar field  $\phi$ , which is a solution of the Einstein equations, is real. Indeed, the relation that makes such a discussion clear is given by Eq. (4). We checked for each model if the CE maximum and minimum points are related to tachyonic solutions and the outcome is discussed in the following.

If the CE global minimum coincides with the  $n$  values that engender real solutions, we have the CE method selecting real brane models. This is the case for all the models analyzed

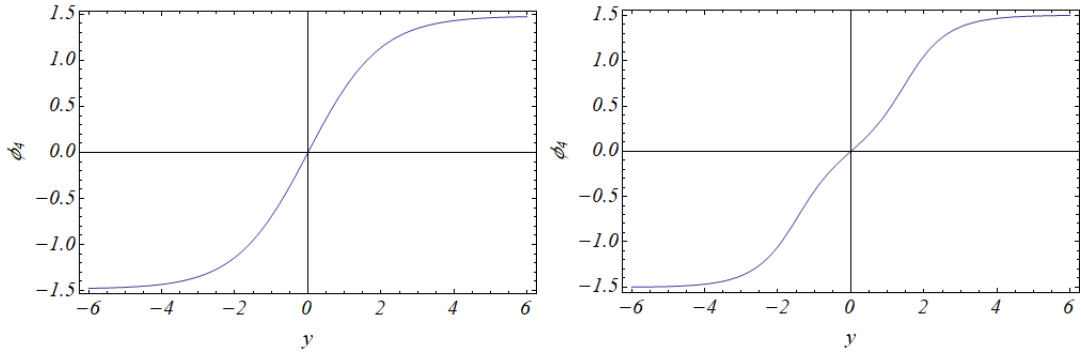


FIG. 10: Brane scalar fields relative to Model 4 considering  $n = 0.82$  (left) and  $n = 1.5$  (right).

in this work. We also analyzed the maximum CE. In this case we find that the maximum CE point for the Model 3 is associated with a tachyonic solution. This could mimic a scenario with unstable solutions decaying for a real stable one, located at the global CE minimum.

It is pertinent to note that considering Model 4 for  $n = 1.5$  we still have a real scalar field solution, but it presents a double-kink structure formation and could be related with the instability of some previous scenario, even if it was not tachyonic.

## VI. CONCLUSIONS

We have worked with the CE as a tool to select among many braneworld scenarios described by a free parameter  $n$ . Considering the graphs displaying the CE as a function of  $n$ , one can always identify a global minimum CE. Moreover, some models present other higher entropy minimum points, i.e. regions where  $\partial(CE)/\partial n = 0$  and  $(\partial^2 CE)/(\partial n)^2 > 0$ , but that does not support the smaller CE minimum value.

Another analysis was developed in order to verify the region where the brane scalar field is a real function or a tachyonic one. This was performed by the analysis of the sign of the warp factor's second derivative; if it is positive, one has tachyonic solutions, otherwise it is real. For the  $n$  values engendering real functions that are also the intervals for low entropy global minimum, the CE is selecting real brane solutions.

We conclude that CE altogether with the warp factor's analysis could be a physical

observable to constraint one single free parameter  $n$ . On the other hand, it does not exclude the possibility of indicating a more intricate scenario where the scalar field could initially be at a potential with higher CE value and then decay to smaller CE minima through symmetry breaking mechanism or even a quantum tunneling process.

It is worth to mention that the expected values for  $n$  according to CE can be further analyzed in different sort of applications. For instance, in a cosmological perspective, the Friedmann-like equations can be constructed for the above braneworld scenarios. It can be checked if the values that CE has indicated for  $n$  in the different models are able to predict healthy cosmological models, say, by describing a late-time accelerated expansion universe [22].

On a more fundamental level, the predicted values for  $n$  presented in this work can be applied to attempt to recover the newtonian potential on a weak gravitational field limit in the brane [14]. Also the possibility of solving the hierarchy problem within these braneworld scenarios with the referred values of  $n$  can be further analysed [7]. All these applications have not been done so far since the braneworld models of Ref.[8] are quite recent. Moreover, with no restrictions for  $n$ , those applications could look artificial. In this way, in possession of the here presented CE results, it is our intent to report on these subjects soon.

- 
- [1] Padmanabhan, T., Phys. Rep. **380**, 235 (2003).
  - [2] Bull, P. *et al.*, Phys. Dark. Univ. **12**, 56 (2016).
  - [3] Sahni, V., Lect. Not. Phys. **653**, 141 (2004).
  - [4] Oman, K.A. *et al.*, Month. Not. Royal. Astron. Soc. **452**, 3650 (2015).
  - [5] Sahni, V., Class. Quant. Grav. **19**, 3435 (2002).
  - [6] L.B. Castro, *et al.*, Journal of Cosmology and Astroparticle Physics **08** (2014) 047.
  - [7] Randall, L. and Sundrum, R., Phys. Rev. Lett. **83**, 3370 (1999).
  - [8] Arkani-Hamed, N. *et al.*, Phys. Lett. B **429**, 263 (1998).
  - [8] Chinaglia, M. and Bernardini, A. E. and da Rocha, R., International Journal of Theoretical Physics **55**, 4605 (2016).
  - [9] Marcelo Gleiser, Nikitas Stamatopoulos, Phys. Lett. **B713**, 304 (2012).
  - [10] R. A. C. Correa, P. H. R. S. Moraes, Eur. Phys. J. C **76**, 100 (2016).
  - [11] A.Goncalves da Silva and Roldão da Rocha, Phy. Lett. B **774** (2017) 38.
  - [12] Nelson R. F. Braga and Roldão da Rocha, Phy. Lett. B **767** (2017) 386.
  - [13] Alex E. Bernardini, Nelson R. F. Braga and Roldão da Rocha, Phy. Lett. B **765** (2017) 81.
  - [14] L. Randall e R. Sundrum, Physical Review Letters **83**, 4690 (1999).
  - [15] V. A. Rubakov, and M. E. Shaposhnikov, Phys. Lett. B **125**, 139 (1983).
  - [16] Bernardini, A. E.; Da Rocha, Roldão, Advances in High Energy Physics **2013**, 1 (2013).
  - [17] D. Bazeia, L. Losano and J. M. C. Malbouisson, Phys. Rev. **D66**, 101701 (2002).
  - [18] Bernardini, A. E.; Chinaglia, M. ; Da Rocha, Roldo, European Physical Journal Plus **130**, 1 (2015).
  - [19] O. Arias, R. Cardenas and I. Quiros, Nucl. Phys. **B643**, 187 (2002).
  - [20] N. Barbosa-Cendejas and A. Herrera-Aguilar, Phys. Rev. **D 73**, 084022 (2006).
  - [21] C. E. Shannon, The Bell System Technical Journal **27** (1948) 379
  - [22] S.J. Perlmutter, *et al.*, Astrophys. J. **517** (1999) 565.
  - [23] R. Rajaraman, *Solitons and Instantons*, (North-Holland, Amsterdam, 1982).
  - [24] E. B. Bogomolnyi, Sov. J. Nucl. Phys. **24**, 489 (1976).

## Appendix A: Deformation procedure

Henceforth we follow [8, 16] in order to present a review of the deformation procedure calculation that can generate topological and non-topological defects described by single real scalar fields  $\psi$ . The main requirement in order to generate such solutions (known as BPS-like solutions [23]) is to impose some features on the potentials that drives the scalar fields. One demand that the potential  $V(\psi)$  generates a set of critical points,  $\{\bar{\psi}_1, \dots, \bar{\psi}_n\}$ , such that  $(dV/d\psi|_{\psi=\bar{\psi}_i} = 0)$  as well as  $V(\bar{\psi}_i) = 0$ , with  $i = 1, 2, \dots, n$ .

As a consequence, deformed potentials will engender two types of defects with different topologies. If the potential has at least two degenerate minima, it engenders two new vacua corresponding to the classical field configurations,  $\psi = \pm\bar{\psi}$ . In one spatial dimension the space boundaries consist in two critical points of the potential, *i.e.* those located at  $x = -\infty$  and  $x = +\infty$  corresponding to the vacua configuration space topology of the fields. In this case, there is an identity map that carries  $x = -\infty$  into  $\psi = -\bar{\psi}$  and  $x = +\infty$  into  $\psi = +\bar{\psi}$ , which defines topological or kink-like structures. On the other hand, if the potential has one single minimum,  $\psi = \bar{\psi}$ , it leads to  $\lim_{x \rightarrow \pm\infty} \psi = \bar{\psi}$ . Consequently, a trivial map carries both boundary spatial points in the same field value,  $-\bar{\psi}$  or  $+\bar{\psi}$ , which defines non-topological or lump-like structures. These last structures exhibit a bell-shaped profile that guarantee integrability as well as matter localization, which has motivated Chinaglia M.; Bernardini A. and Roldão R. to use them as input to build up novel warp factor structures of braneworlds in [8].

A cyclic deformation method was developed in [16] attempting to derive topological and non-topological solutions without the need to solve second order differential equations [16]. A triggering primitive defect known *a priori* departs the chain. Given that, one is able to construct an  $N+2$ -cyclic deformation chain through the application of a chain rule constrained by hyperbolic and trigonometric fundamental relations. The initial scalar field solution was identified by the  $\lambda\chi^4$  among other solutions in [16] and by the Sine-Gordon in [18]. Therefore, we will use the Greek letter  $\chi$  for the triggering known solution and  $\psi$  for the deformed defects.

Note that, although these chains can generate kinks and lumps, Chinaglia, Bernardini e da Rocha have used just some of the lump solutions in order to build up the brane scenarios.

The generalized  $\lambda$ -deformation operation, with  $\lambda = 0, 1, 2, \dots, N$  is effectuated by the



$\lambda$ -derivative given by

$$g^{[\lambda]}(\psi^{[\lambda]}) = \frac{d\psi^{[\lambda]}}{d\psi^{[\lambda-1]}}, \quad (\text{A1})$$

where  $\psi^{[\lambda]}$  are real scalar fields corresponding to defect structures built from an  $N+2$ -cyclic deformation chain triggered by  $\chi \equiv \chi(y) \sim \psi^{[-1]}$ , such that one effectively has  $\psi^{[\lambda]} \equiv \psi^{[\lambda]}(\chi)$ .

The hyperbolic deformation chain [16] is given by

$$\begin{aligned} \psi_\chi^{[0]} &= \tanh(\chi), \\ \psi_\chi^{[1]} &= \tanh(\chi) \operatorname{sech}(\chi), \\ \psi_\chi^{[2]} &= \tanh(\chi) \operatorname{sech}(\chi)^2, \\ &\vdots \\ \psi_\chi^{[N-1]} &= \tanh(\chi) \operatorname{sech}(\chi)^{N-1}, \\ \psi_\chi^{[N]} &= \operatorname{sech}(\chi)^N, \end{aligned} \quad (\text{A2})$$

where the subindex denotes the corresponding derivative, which upon straightforward integrations leads to

$$\begin{aligned} \psi^{[0]}(\chi) &= \ln[\cosh(\chi)], \\ \psi^{[1]}(\chi) &= -\operatorname{sech}(\chi), \\ \psi^{[2]}(\chi) &= -\frac{1}{2} \operatorname{sech}(\chi)^2, \\ &\vdots \\ \psi^{[N-1]}(\chi) &= -\frac{1}{N-1} \operatorname{sech}(\chi)^{N-1}, \\ \psi^{[N]}(\chi) &= \sinh(\chi) {}_2F_1\left[\frac{1}{2}, \frac{1+N}{2}, \frac{3}{2}, -\sinh(\chi)^2\right], \end{aligned} \quad (\text{A3})$$

where  ${}_2F_1$  is the Gauss' hypergeometric function and the arbitrary integration constants have been suppressed, since they are not effective in this framework.

From Eqs. (A2-A3) one identifies

$$g^{[\lambda]}(\psi^{[\lambda]}) = \operatorname{sech}(\chi) \equiv \exp[-\psi^{[0]}], \quad \lambda = 1, 2, \dots, N-1, \quad (\text{A4})$$

$$g^{[N]}(\psi^{[N]}) = 1/\sinh(\chi), \quad (\text{A5})$$

and

$$\prod_{\lambda=1}^{N-1} g^{[\lambda]}(\psi^{[\lambda]}) = \frac{d\psi^{[N-1]}}{d\psi^{[0]}} = \operatorname{sech}(\chi)^{N-1} \equiv \exp[-(N-1)\psi^{[0]}], \quad (\text{A6})$$

from which the complete expression for the chain rule of the  $N+2$ -cyclic deformation can be written as

$$\frac{d\psi^{[0]}}{d\chi} \prod_{\lambda=1}^N g^{[\lambda]}(\psi^{[\lambda]}) \frac{d\chi}{d\psi^{[N]}} = 1, \quad (\text{A7})$$

from which  $N+2$  deformation functions closing the cycles can be identified.

By assuming a parametrization in terms of generalized BPS functions [24], one has

$$\begin{aligned} y_{\psi^{[\lambda]}}^{[\lambda]} &= \frac{d\psi^{[\lambda]}}{ds} = y_{\psi^{[\lambda-1]}}^{[\lambda-1]} g^{[\lambda]}(\psi^{[\lambda]}) = y_{\psi^{[\lambda-r]}}^{[\lambda-r]} g^{[\lambda-r+1]}(\psi^{[\lambda-r+1]}) \\ &= w_\chi \psi_\chi^{[\lambda]}, \end{aligned} \quad (\text{A8})$$

with  $w_\chi = d\chi/ds$ . In this case, the constraint equation is written as

$$\begin{aligned} \sum_{\lambda=0}^{N-1} (y_{\psi^{[\lambda]}}^{[\lambda]})^2 &= (y_{\psi^{[0]}}^{[0]})^2 \sum_{\lambda=0}^{N-1} \left( \frac{d\psi^{[\lambda]}}{d\psi^{[0]}} \right)^2 \\ &= w_\chi^2 \sum_{\lambda=0}^{N-1} (\psi_\chi^{[\lambda]})^2 = w_\chi^2 \tanh(\chi)^2 \sum_{\lambda=0}^{N-1} (\text{sech}(\chi))^{2\lambda} \\ &= w_\chi^2 \tanh(\chi)^2 \frac{1 - \text{sech}(\chi)^{2N}}{1 - \text{sech}(\chi)^2} = w_\chi^2 \left( 1 - \text{sech}(\chi)^{2N} \right) \\ &= w_\chi^2 [1 - (\psi_\chi^{[N]})^2] = w_\chi^2 - (y_{\psi^{[N]}}^{[N]})^2, \end{aligned} \quad (\text{A9})$$

which leads to

$$\sum_{\lambda=0}^N (y_{\psi^{[\lambda]}}^{[\lambda]})^2 = w_\chi^2. \quad (\text{A10})$$

Therefore the preliminary relevant result reported on [16] is that the topological masses follow the constraint given by

$$\sum_{\lambda=0}^N (M^{\psi^{[\lambda]}}) = M^\chi. \quad (\text{A11})$$

Following the above framework, also a trigonometric deformation chain [16] can be obtained by concomitantly changing  $\tanh(\chi) \mapsto -\sin(\chi)$  and  $\text{sech}(\chi) \mapsto \cos(\chi)$  into Eqs. (A2-

A3), such that

$$\begin{aligned}
\psi^{[0]}(\chi) &= \cos(\chi), \\
\psi^{[1]}(\chi) &= \frac{1}{2} \cos(\chi)^2, \\
\psi^{[2]}(\chi) &= \frac{1}{3} \cos(\chi)^3, \\
&\vdots \\
\psi^{[N-1]}(\chi) &= \frac{1}{N} \cos(\chi)^N, \\
\psi^{[N]}(\chi) &= -\frac{\cos(\chi)^{N+1}}{N+1} {}_2F_1\left[\frac{1+N}{2}, \frac{1}{2}, \frac{3+N}{2}, \cos(\chi)^2\right].
\end{aligned} \tag{A12}$$

It results into a set of constraints analogous to those described by Eqs. (A10-A11).

Here we present two of the primitive chosen kink solutions (known *a priori*)

$$\chi_a(y) = \tanh(y) \quad (\lambda\chi^4 \text{ model}), \tag{A13}$$

$$\chi_b(y) = \text{sech}(y), \tag{A14}$$

that shall have triggered off the CDC depicted from  $n + 2$ -cyclic chains (with  $n = 1$  and  $n = 2$ ) in Refs. [16] which generate the lump solutions inserted to calculate the brane scenarios in [8] that are analyzed in the present work.

Deformed defects derived from  $\chi_a$  and  $\chi_b$  holding a lump-like behavior,  $\psi_1, \psi_2, \psi_3$  and  $\psi_4$ , were identified with  $A(y)$  from Eq. (5), as to support warp factors that generate consistent braneworld scenarios driven by a scalar field  $\phi$  as set by the action from (1). In Table II we present the expression for the four lump deformed defects [16], inserted as ansatz on Eq.(5). In order to result in the lumps  $\psi_1, \psi_2$  and  $\psi_3$ , the CDC was triggered by the known solution  $\chi_a = \tanh(y)$ . However, the 4-cyclic trigonometric result,  $\psi_4$ , was derived considering the triggering function  $\chi_b = \text{sech}(y)$ .

Chain	Deformation function	Deformed lump solution
3-cyclic	Hyperbolic	$\psi_1 = \frac{-\ln[\cosh[n \tanh(y)] \operatorname{sech}(n)]}{n}$
3-cyclic	Trigonometric	$\psi_2 = \frac{\cos[n \tanh(y)] - \cos(n)}{n}$
4-cyclic	Hyperbolic	$\psi_3 = \frac{(\operatorname{sech}[n \tanh(y)] - \operatorname{sech}(n))}{n}$
4-cyclic	Trigonometric	$\psi_4 = \frac{(2n \operatorname{sech}(y) + \sin[2n \operatorname{sech}(y)])}{4n}$

TABLE I: Lump-like deformed defects derived with hyperbolic and trigonometric functions in a CDC triggered by a solution known *a priori* [16].